



Fast and robust control of nanopositioning systems: Performance limits enabled by field programmable analog arrays

Mayank Baranwal, Ram S. Gorugant, and Srinivasa M. Salapaka

Citation: *Review of Scientific Instruments* **86**, 085004 (2015); doi: 10.1063/1.4929379

View online: <http://dx.doi.org/10.1063/1.4929379>

View Table of Contents: <http://scitation.aip.org/content/aip/journal/rsi/86/8?ver=pdfcov>

Published by the AIP Publishing

Articles you may be interested in

[Ultrafast feedback-controlled electromigration using a field-programmable gate array](#)

J. Vac. Sci. Technol. B **33**, 02B106 (2015); 10.1116/1.4903929

[An experimental comparison of proportional-integral, sliding mode, and robust adaptive control for piezo-actuated nanopositioning stages](#)

Rev. Sci. Instrum. **85**, 055112 (2014); 10.1063/1.4876596

[Robust adaptive variable speed control of wind power systems without wind speed measurement](#)

J. Renewable Sustainable Energy **5**, 063115 (2013); 10.1063/1.4840035

[Digital control of force microscope cantilevers using a field programmable gate array](#)

Rev. Sci. Instrum. **79**, 123705 (2008); 10.1063/1.3043432

[Digital field programmable gate array-based lock-in amplifier for high-performance photon counting applications](#)

Rev. Sci. Instrum. **76**, 093112 (2005); 10.1063/1.2008991

An advertisement for Janis Dilution Refrigerators & Helium-3 Cryostats for Sub-Kelvin SPM. On the left, there is a photograph of a complex scientific apparatus, likely a dilution refrigerator or cryostat, showing various tubes, coils, and mechanical components. To the right of the image, the word "JANIS" is written in a large, bold, white, sans-serif font. Below "JANIS", the text "Janis Dilution Refrigerators & Helium-3 Cryostats for Sub-Kelvin SPM" is displayed in a white, bold, sans-serif font. At the bottom, the text "Click here for more info www.janis.com/UHV-ULT-SPM.aspx" is shown in a white, bold, sans-serif font.

Fast and robust control of nanopositioning systems: Performance limits enabled by field programmable analog arrays

Mayank Baranwal,^{a)} Ram S. Gorugantu,^{b)} and Srinivasa M. Salapaka^{c)}

Department of Mechanical Science and Engineering, University of Illinois at Urbana-Champaign, Urbana, Illinois 61801, USA

(Received 20 May 2015; accepted 11 August 2015; published online 27 August 2015)

This paper aims at control design and its implementation for robust high-bandwidth precision (nanoscale) positioning systems. Even though modern model-based control theoretic designs for robust broadband high-resolution positioning have enabled orders of magnitude improvement in performance over existing model independent designs, their scope is severely limited by the inefficiencies of digital implementation of the control designs. High-order control laws that result from model-based designs typically have to be approximated with reduced-order systems to facilitate digital implementation. Digital systems, even those that have very high sampling frequencies, provide low effective control bandwidth when implementing high-order systems. In this context, field programmable analog arrays (FPAAs) provide a good alternative to the use of digital-logic based processors since they enable very high implementation speeds, moreover with cheaper resources. The superior flexibility of digital systems in terms of the implementable mathematical and logical functions does not give significant edge over FPAAs when implementing linear dynamic control laws. In this paper, we pose the control design objectives for positioning systems in different configurations as optimal control problems and demonstrate significant improvements in performance when the resulting control laws are applied using FPAAs as opposed to their digital counterparts. An improvement of over 200% in positioning bandwidth is achieved over an earlier digital signal processor (DSP) based implementation for the same system and same control design, even when for the DSP-based system, the sampling frequency is about 100 times the desired positioning bandwidth. © 2015 AIP Publishing LLC. [<http://dx.doi.org/10.1063/1.4929379>]

I. INTRODUCTION

Nanopositioning forms one of the primary requirements of many high-impact applications such as scanning probe microscopy, semiconductor test equipment, in synchrotrons for x-ray microscopy, and in molecular biology studies. Typically, the nanopositioning devices¹ comprise flexure based stages which are actuated by piezoelectric materials. The advantages of these devices are several: they provide repeatable sub-nanometer motion, do not have backlash, do not suffer from wear and tear, require very little maintenance, can generate large forces, are operable in a wide range of temperatures, and are not affected by magnetic fields. The main challenges arise from the inherent dynamics of the flexure stages, nonlinear effects of piezoactuation such as hysteresis and creep and effects of measurement noise, model parameter uncertainties, and disturbance from the surroundings that are difficult to model.

There have been several approaches to improve the speed, resolution, and accuracy of nanopositioning systems. These include—feedforward control designs,^{8,14} using charge amplifiers instead of voltage amplifiers to reduce hysteresis,⁶ and feedback control designs with large gains at low frequen-

cies.^{9,28} While feedforward controllers can be designed to reject certain nonlinear effects such as hysteresis,^{7,8} such schemes fail to cope up with various unmeasured input disturbances, thereby resulting in poor output performance. On the other hand, implementations of feedback control designs have resulted in positioning resolution being practically independent of piezoelectric nonlinearities, where their effects become negligible compared to measurement noise. Furthermore, appropriate feedback designs are less sensitive to uncertainties in operating conditions than their feedforward counterparts. Commercial feedback schemes are typically based on PI/PII designs. However, as shown in Ref. 27, such PI-based schemes fail to meet the bandwidth requirements for positioning. The feedback control framework presented in Refs. 18 and 27 determines and quantifies trade-offs between performance objectives, assesses if desired specifications are feasible, and provides a way to design controllers to achieve specifications when possible. In Ref. 27, this framework had resulted in a significant improvement by over 40 times for similar stability margins when compared to proportional-integral/proportional-integral-derivative (PI/PID) based design prevalent in the industry.

Motivated by the distinct advantages of both *model-based* feedforward and feedback schemes and the inherent multi-objective aspect of this control problem, more recently, two-degrees-of-freedom (2DOF), *optimal* control design framework^{17–19,30,35} is being employed where the regular feedback control is appended with a feedforward scheme for the

^{a)}Author to whom correspondence should be addressed. Electronic mail: baranwa2@illinois.edu. URL: <http://web.engr.illinois.edu/~baranwa2>.

^{b)}gorugan2@illinois.edu

^{c)}salapaka@illinois.edu. URL: <http://web.engr.illinois.edu/~salapaka/mechse>.

reference signal to meet stricter performance specifications. For example, in Ref. 18, the authors have analyzed fundamental trade-offs between positioning resolution, tracking bandwidth, and robustness to modeling uncertainties in 2DOF control designs for nanopositioning systems. The authors achieve as high as 330% increase in bandwidth for a 2DOF control architecture for similar robustness and resolution over optimal feedback-only designs. However, the main bottleneck is the implementation of such high-order controllers. For example, in Ref. 18, even with very high-speed digital signal processors (DSPs) (sampling freq. ~ 100 kHz), the authors were forced to implement reduced-order controllers, thereby resulting in a non-optimal controller performance.

The advent of reconfigurable computing devices, such as complex programmable logic devices (CPLDs) and field programmable gate arrays (FPGAs), has given a new dimension to signal processing applications;¹⁵ not only they allow users to customize the hardware to suit the specific requirements but also enable high speed applications. More recently, field programmable analog arrays (FPAA) have emerged as interesting alternatives to most signal processing based applications.⁴ Even though the use of FPAA devices is still limited due to small number of suppliers, a growing interest in using FPAAAs for various engineering applications is expected.¹²

In FPAAAs, a fully differential switched capacitor architecture² allows integration of a larger number of elements per chip; high precision and high efficiency gain when compared to DSP processors. The main popularity of FPGA based implementations stems from the flexibility that digital systems provide compared to their analog counterparts. However, implementing FPGA based systems requires considerable experience and familiarity and expertise in terms of allocation of resources (computing units) to the tasks at hand. More importantly, they inherit the disadvantages of discretization of analog systems from sampling (such as aliasing) and imperfections in converting digital signals to the analog signals. Recent advances in FPAAAs have resulted in increasingly flexible systems that can accommodate a large set of mathematical operations. It is relatively simple to implement transfer functions using FPAAAs with reconfigurable networks of op-amps based circuits; moreover, FPAA technology is relatively very inexpensive. Although, a direct comparison between FPAA and FPGA implementations is impossible; in this paper, we bring out the differences between them in terms of implementing for a specific, although important, applications to precision (nano) positioning in atomic force microscopy (AFM),³¹ especially with growing interest in high speed nanoimaging.

This paper aims at enabling high-bandwidth positioning to facilitate high-speed imaging in AFM. High speed nanoimaging has many applications including imaging of dynamic biomolecular processes.³ High-bandwidth demands on positioning require high clock-speed/sampling frequency from digital implementation platforms such as FPGA. These requirements become severe as the controller order increases. For instance, digital implementation of a 10th order controller may require ten times higher sampling frequency than for a typical third order implementation. In contrast, analog (FPAA) based implementations require no sampling and bandwidths of up to 400 kHz can be easily achieved.

In this work, we explore model-based optimal control designs for the X-Y nanopositioning system for different application scenarios on an MFP3D AFM and experimentally implement these using FPAA devices. Specifically, we consider control designs similar to those in Refs. 18 and 19. The implementation of these designs using the FPAA has resulted in a significant improvement (by about 200%) in tracking bandwidths when compared to earlier DSP²⁶ based implementation of similar control design, which themselves are about 9 times faster than an exhaustively tuned PI/PII designs, prevalent in commercial systems.^{18,27}

This paper is organized as follows. In Section II, we present the objectives and challenges in high speed control of positioning systems. In Section III, we present various control schemes that we have implemented on the piezo-stage system. In Section IV, we give details of implementation on the FPAA and experimental results. We also motivate the use of FPAAAs by highlighting the limitations of a high-end DSP²⁶ for a model-based control design. Finally, in Section V, we present the conclusions and future work.

II. OBJECTIVES AND CHALLENGES

A typical nanopositioning system comprises of a flexure stage and actuators (typically piezoelectric) and/or sensors along with the feedback system. We present our analysis and design in terms of transfer function block diagrams as shown in Fig. 1. In this figure, G is the transfer function of the scanner comprising the actuator, flexure stage, and the sensor. It represents the dynamical relationship between its output, the flexure stage displacement y , and its input, the voltage u given to the actuator. The signals d , n , and r represent noise due to unmodeled dynamics, sensor noise, and the command signal that a positioning system needs to track, respectively.

In an open-loop positioning system, where the sensor signal is not fed back to the controller, the performance is severely limited by mechanical noise such as drift, creep, and hysteresis. Including their precise behavior in device models is practically infeasible and hence they are treated as noise. Therefore, feedback based schemes are employed to compensate for the mechanical noise at the cost of relatively small sensor noise.

As discussed in Ref. 18, the performance of a nanopositioning system is characterized by its resolution, tracking bandwidth, and robustness to modeling uncertainties. The main objective for the design of the controller K is to make the tracking error small and simultaneously attenuate sensor noise to achieve high resolution. This is achieved by posing a

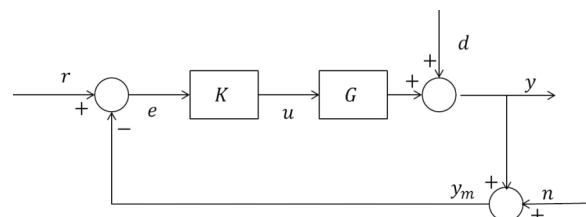


FIG. 1. Block diagram schematic for nanopositioning systems.

model-based multi-objective optimization framework, where the required objectives are described in terms of norms of the corresponding transfer functions, as described below.

From Fig. 1, we have

$$\begin{aligned} \text{Tracking error, } e &= (1 + GK)^{-1}(r - n) = S(r - n), \\ \text{Output displacement, } y &= GKe = T(r - n), \\ \text{Control input, } u &= Ke = KS(r - n), \\ S &= 1/(1 + GK), \\ T &= GK/(1 + GK), \end{aligned} \quad (1)$$

where the sensitivity transfer function, S , is the closed-loop transfer function from reference r to tracking error e , and the complementary sensitivity transfer function, T , is the closed-loop transfer function from reference r to the displacement y . It can be shown that the ratio of percentage change in output displacement to percentage change in model parameters is equal to the sensitivity transfer function, i.e., $\frac{dy/y}{dG/G} = S$. Therefore, S is a measure of robustness of the closed-loop system to modeling and parametric plant uncertainties. The bandwidth ω_B is the frequency where Bode plot of the sensitivity transfer function crosses the -3 dB line. There are fundamental limitations on the achievable specifications, which regardless of the control design cannot be overcome. For instance, due to the algebraic constraint, $S + T = 1$, increasing ω_B would mean that T would still be large for relatively higher frequencies. Because T represents the closed-loop transfer function from noise n to displacement y , this would result in significant amplification of high-frequency noise, thereby resulting in poor tracking performance. Similar to ω_B , ω_{BT} is the bandwidth based on the complementary sensitivity transfer function T , defined by its crossing of the -3 dB line. For better resolution, i.e., better noise mitigation, ω_{BT} should be small.

Similarly, KS is the closed-loop transfer function from tracking error e to controller output u . KS needs to be bounded so that the controller output u is bounded. Since in case of MFP-3D, the maximum absolute voltage the piezo-actuators provide is ≈ 10 V, it is important to bound the controller output to avoid signal saturation and its effects.

In the context of nanopositioning systems, most applications impose high demands on positioning resolution and tracking bandwidths. Other challenges include nonlinear flexure stage dynamics that limit the bandwidth of the positioning stage and nonlinearities in piezoactuation such as hysteresis and creep that are difficult to model. Using modern control techniques, most of these challenges have been addressed.^{18,19,25,29} However, the bottleneck is in the hardware implementation of the control schemes, which demand very high sampling frequencies. In this work, we address this issue by the use of FPAs, which allow analog implementation of the controllers.

III. OPTIMAL CONTROL DESIGN SCHEMES FOR NANOPOSITIONING SYSTEMS

In this work, we have focused on high-bandwidth, high-resolution, and reliable positioning. The design of control

laws for achieving *simultaneously* above objectives renders tuning-based control designs (PI/PII) impractical and ineffective. Hence, we employ modern robust control theoretic framework, where an optimization problem over a set of proper, stabilizing controllers, \mathcal{K} is posed for a given set of design specifications and when feasible, results in an optimal control law K . The main advantage of this approach is that the performance objectives can be directly incorporated into the cost function. These optimization problems are of the form,

$$\min_{K \in \mathcal{K}} \|\Phi(K)\|_\infty, \quad (2)$$

where Φ is a matrix transfer function whose elements are in terms of the closed-loop transfer functions in (1). For example, Φ represents a matrix transfer function from *external* variables, such as reference command r and sensor noise n , to *regulated* outputs, such as tracking error e and control signal u . In this case, minimizing $\|\Phi\|_\infty$ is equivalent to making the ratio of the magnitudes of regulated variables to external variables small, regardless of the external signals (i.e., the optimization problem seeks to minimize the worst case gain from disturbance inputs to system outputs). More specifically, in this section, we present control designs for the above goals using (1) 2DOF \mathcal{H}_∞ framework, (2) 2DOF model-matching framework,¹⁸ and (3) 2DOF Glover-McFarlane robustifying framework.¹³

Remark: These optimization problems have been studied extensively^{10,33} and can be solved efficiently using standard MATLAB²² routines.

A. 2-DOF \mathcal{H}_∞ control

The feedback-only scheme has certain performance limitations, which can be alleviated by using a 2DOF architecture shown in Fig. 2(a).^{18,19}

In contrast to the feedback-only scheme, where the controller acts only on the difference between the reference r and the position-measurement y_m , in the 2DOF scheme, the controller acts independently on them. The generalized plant for a 2DOF \mathcal{H}_∞ control framework is shown in Fig. 2(b). From Fig. 2(a),

$$\begin{aligned} \text{Tracking error, } e &= S_{er}r + T_n, \\ \text{Position, } y &= T_{yr}r - T_n, \\ \text{Control signal, } u &= S(K_{ff} + K_{fb})r - SK_{fb}n, \\ S_{er} &= S(1 - GK_{ff}), \\ T_{yr} &= SG(K_{ff} + K_{fb}). \end{aligned}$$

The signals $W_S e$, $W_u u$, and $W_T y$ represent tracking error, the noise component in the position signal, and the control signal, respectively, where the weights W_S , W_T , and W_u are chosen to reflect the design specifications of tracking bandwidth, positioning resolution, and saturation limits on the control signal. To achieve these objectives, a control design K which minimizes the \mathcal{H}_∞ -norm of the transfer function from w to z is sought through the optimal control problem. \mathcal{H}_∞ -norm is the maximum singular value of a transfer function over the space of matrix-valued functions that are bounded in the open right-half of the complex plane defined by $Re(s) > 0$.

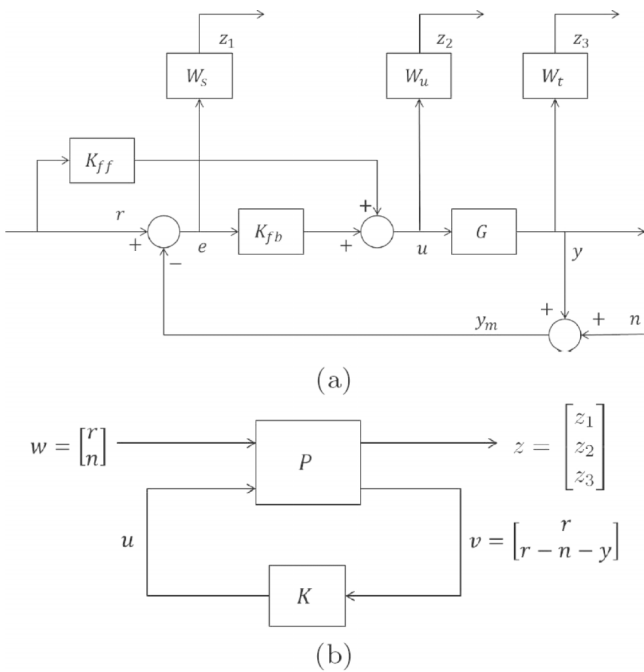


FIG. 2. A 2DOF \mathcal{H}_∞ control architecture. (a) A control architecture with both *feedforward* and *feedback* controllers— K_{ff} and K_{fb} . The control design specifications are expressed using weighting functions W_s , W_T , and W_u . (b) The control problem is then posed as a mathematical optimization problem seeking minimum of the \mathcal{H}_∞ -norm of the generalized plant, P . The solution to this optimization problem results in an optimal stabilizing controller $K = [K_{ff} \ K_{fb}]^T$.

The optimization problem then is to solve for all stabilizing controllers K posed in the stacked sensitivity framework,

$$\min_{K \in \mathcal{K}} \left\| \begin{matrix} W_s S \\ W_u K S \\ W_t T \end{matrix} \right\|_\infty, \quad (3)$$

where \mathcal{K} is a set of all stabilizing controllers. This optimization problem is solved using standard MATLAB routines. The feedback-only control scheme is indeed a special case of the 2DOF scheme, where $K_{ff} = 0$. The control objectives translate to small roll-off frequency as well as high roll-off rates for T to have good resolution, a long range of frequencies for which S_{er} is small to achieve large bandwidth, and low (near 1) values of the peak in the magnitude plot of $S(j\omega)$ for robustness to modeling uncertainties.²⁹ The optimization problem is to find stabilizing controllers $K = [K_{ff} \ K_{fb}]^T \in \mathcal{K}$ such that the \mathcal{H}_∞ -norm of the regulated output z is minimized.

B. 2DOF model-matching control

Some nanopositioning systems have pre-designed feedback component K_{fb} , which cannot be replaced or changed. However, typically, there are no such restrictions on the feedforward control design since it can be easily implemented as a prefilter on the reference signal. The prefilter K_{pre} is chosen so that the closed-loop transfer function T mimics the reference transfer function T_{ref} (Fig. 3). Desired transient characteristics such as settling time and overshoot can be

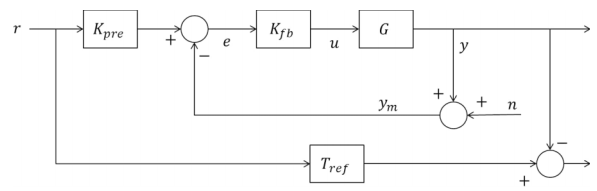


FIG. 3. Model matching through the prefilter problem.

incorporated by choosing the appropriate model T_{ref} , and since the closed-loop device is designed to mimic the model, it inherits the transient characteristics too. If T is the original complementary sensitivity transfer function with the feedback-only component, the mismatch error signal from Fig. 3 is given by $e = (T_{ref} - TK_{pre})r$. Hence, minimizing the mismatch error signal is equivalent to

$$\min_{K_{pre} \in \mathcal{K}} \|E(s)\|_\infty = \min_{K_{pre} \in \mathcal{K}} \|T_{ref} - TK_{pre}\|_\infty, \quad (4)$$

where \mathcal{K} is a set of all stabilizing controllers. If T is minimum phase with no RHP (right half plane) zeros, this optimization problem is trivial and the optimal prefilter $K_{pre} = T^{-1}T_{ref}$. However, typical nanopositioning systems are flexure based with non-collocated actuators and sensors, which typically manifest as non-minimum phase zeros of T . In this case, the optimal solution can be found by applying NP (Nevanlinna-Pick) theory described in Ref. 10.

C. 2DOF Optimal robust model matching control

Even though some nanopositioning systems with pre-designed feedback controllers exhibit satisfactory resolution and tracking bandwidth when operated at “near optimal” operating conditions, a slight deviation from these operating conditions may result in rapid degradation in tracking performance sometimes resulting in system instability. For such systems, robustness is a major concern. In Ref. 32, Glover-McFarlane method^{13,23} that wrapped around pre-existing controllers was implemented that resulted in significant improvements in robustness. In the current work, we use a 2DOF control design developed in Refs. 16 and 20 to simultaneously design a wrap-around feedback controller for robustness as well as the feedforward controller for better bandwidth. Fig. 4(a) shows the optimal 2DOF robust control architecture. The plant $G_s = GK_s$ is the shaped plant with K_s being the pre-existing controller. The optimization routine seeks $K = [K_r \ K_y]$ such that the closed-loop system guarantees “optimal” robustness to modeling uncertainties as well as minimizing the mismatch between the transfer function from r to y and a reference transfer function T_{ref} . The robustness condition is imposed by requiring the controller to guarantee stability for a set of transfer function models that are “close” to the nominal model G_s . The resulting optimal controller guarantees the stability of the closed-loop positioning system where the shaped-plant is represented by *any* transfer function G_p in the set,

$$\{G_p = (M - \Delta_M)^{-1}(N + \Delta_N), \|\Delta_M \ \Delta_N\|_\infty \leq \gamma^{-1}\}, \quad (5)$$

where $G_s = M^{-1}N$ is a coprime factorization,³⁴ $[\Delta_M \ \Delta_N]$ represents the uncertain dynamics, and γ specifies a bound

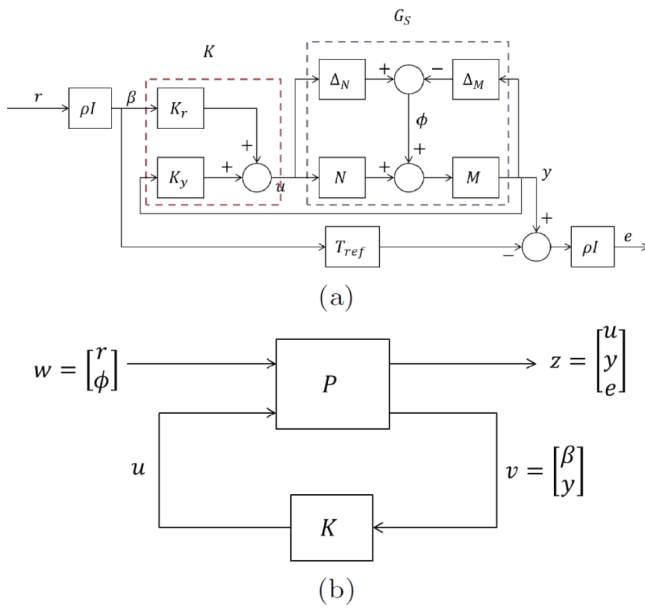


FIG. 4. A 2DOF optimal robustifying controller architecture. (a) 2DOF Glover-McFarlane control framework. Uncertainties in the plant are represented by $\Delta = [\Delta_M \ \Delta_N]$ and T_{ref} represents the reference transfer function. ρ is a scalar parameter that captures the relative importance between robustness and model-matching. For $\rho = 0$, the problem reverts to standard 2DOF \mathcal{H}_∞ optimization problem described earlier. (b) Generalized plant for optimal 2DOF robust model matching controller.

on this uncertainty. This characterization of uncertainty is particularly relevant to nanopositioning systems which typically have very low damping; uncertainties in plant parameters for such systems are well addressed by the uncertainty set in Equation (5). Fig. 4(b) shows the generalized plant for 2DOF optimal control robust control framework. The regulated output in this case is $z = [u^T \ y^T \ e^T]^T$ and the controller K is sought to minimize the \mathcal{H}_∞ -norm of the transfer function Φ_{zw} from $w = [r^T \ \phi^T]^T$ to z , as shown in Fig. 4(a), described by

$$\begin{bmatrix} u \\ y \\ e \end{bmatrix} = \begin{bmatrix} \rho K_r S & | & K_y S M^{-1} \\ \rho G_s K_r S & | & S M^{-1} \\ \rho^2 (G_s K_r S - M_0) & | & \rho S M^{-1} \end{bmatrix} \begin{bmatrix} r \\ \phi \end{bmatrix}, \quad (6)$$

where $S = (1 - G_s K_y)^{-1}$ and the exogenous signal ϕ represents a disturbance signal due to the unmodeled dynamics.

IV. CONTROLLER IMPLEMENTATION ON FPAAS AND EXPERIMENTAL RESULTS

A. Hardware description

1. X-Y nanopositioning system

Fig. 5(a) shows the schematic of the X-Y nanopositioning system (MFP-3D X-Y scanner). The scanner has two flexure components with component “X” stacked over “Y” where the sample holder is carried by the X-component. Both stages can deform under the application of force, thereby providing the required motion. These forces are generated using stacked-piezos. The motion of each flexure component is measured by the corresponding nanopositioning sensors.

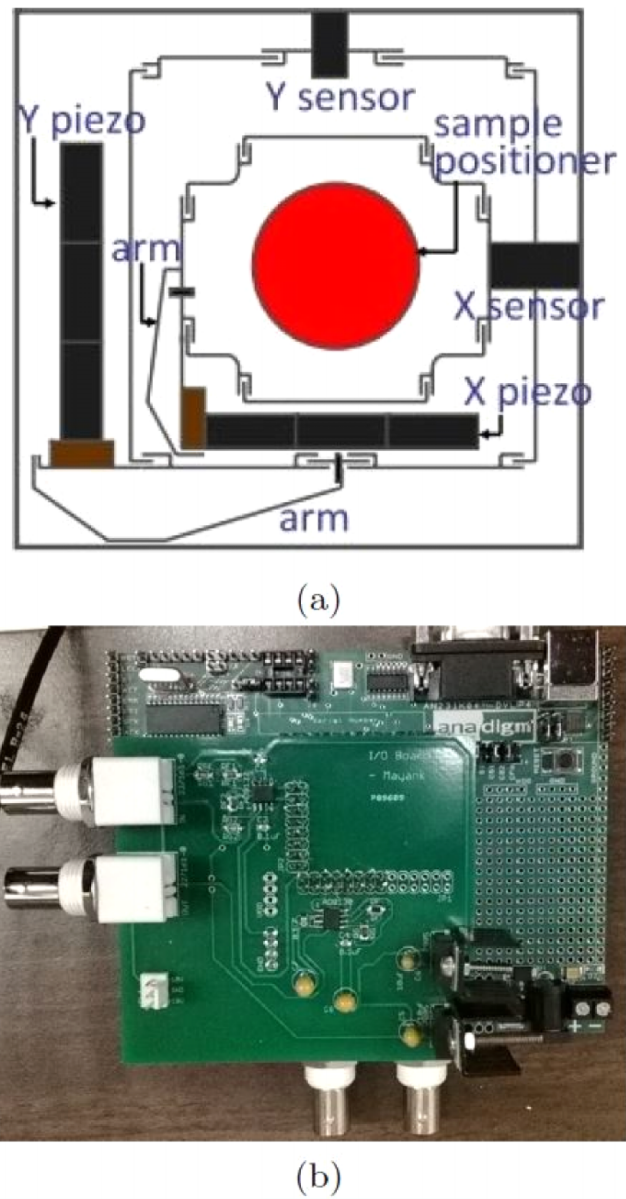


FIG. 5. Associated hardware for nanopositioning control. (a) Schematic of the MFP-3D flexure scanner and (b) a custom designed PCB for interfacing FPAAs with the nanopositioning stage.

which are modified from the linear variable differential transformer (LVDT) and the associated demodulation circuit. The piezoactuators lead to a travel range of $90 \mu\text{m}$ in closed loop in both directions. The nanopositioning sensors have noise less than 0.6 nm (deviation) over $0.1\text{--}1 \text{ kHz}$ bandwidth.

2. FPAAs

The controllers are implemented using FPAAs, which have a direct bandwidth advantage over a very high-performance DSP.²⁶ We now give an analysis for estimating sampling frequency requirements for a DSP implementation. The equations describing the dynamics of a linear controller of order n_c are given by

$$\begin{aligned} x(t + \tau_s) &= Ax(t) + Bu(t), \\ y(t + \tau_s) &= Cx(t + \tau_s) + Du(t), \end{aligned} \quad (7)$$

where $A \in \mathbb{R}^{n_c \times n_c}$, $B \in \mathbb{R}^{n_c}$, $C \in \mathbb{R}^{1 \times n_c}$, and $D \in \mathbb{R}$ are controller parameters; $x \in \mathbb{R}^{n_c}$ represents its state; τ_s is the sampling time-period; and $u(t)$ and $y(t)$ represent its input and output, respectively. Since we have two such controllers in a 2DOF setup, each iteration on DSP roughly requires $2(n_c + 1)^2$ multiplications and as many summations. Our DSP+FPGA based processor P25M²⁶ has an internal clock that runs at 225 MHz. Moreover, the latencies for a 16-bit floating point multiplication are 5 clock cycles and a summation operation has a typical latency of 2 clock cycles. Since the nanopositioning stages under consideration are identified as 9th or 10th-order plants, a simple computation shows that for a 9th-order, 2DOF setup, the maximum allowable *theoretical* sampling speed is roughly 150 kHz, which is 1500 times slower than FPGA clock rate. Moreover, additional clocks are required to execute instructions pertaining to analog inputs/outputs and other useful loop instructions, not forgetting the various saturation conditions for the controller outputs. In practice, we only achieved a maximum of 30 kHz sampling rate for a 2DOF, 9th-order control setup. Since the nanopositioning devices under consideration have resonant frequencies in order of 1-2 kHz, it is not recommended to have a sampling frequency lower than 25-30 kHz. Thus, even a very high-performance DSP can only support reduced order controllers of up to 9th-order. This issue can be alleviated using FPAs, which have implementation bandwidths up to 400 kHz, as is confirmed by the successful implementation of a 13th-order, 2DOF controller resulting in a 200% improvement in tracking bandwidth (for more details, please refer to Sec. IV F).

FPAAs² offers direct realization of very high bandwidth controllers (~400 kHz) by employing AnadigmDesigner2 EDA software. The software allows designer to construct complex analog functions using configurable analog modules (CAMs) as building blocks. With easy-to-use drag-and-drop interface, the design process can be measured in minutes allowing complete analog systems to be built rapidly, simulated immediately, and then downloaded to the FPAAs chip for testing and validation. A custom designed printed-circuit-board (PCB) (see Fig. 5(b)) is used to interface single-ended ± 10 V AFM signals with 0–3.3 V differential signals referenced at 1.5 V. This is achieved by using operational amplifiers AD-8130 and AD-8132 (Analog Devices, Norwood, MA, USA) to scale and convert differential signals to single-ended signals and vice versa.

B. System identification

To identify the dynamics of the positioning systems in our lab, we adapt the well-known blackbox identification method.²¹ A sine sweep signal, over a desired frequency range, is provided to the system and the LVDT sensor output is measured. A linear parametric model is then fitted to this experimental input-output data. The frequency response based identification was done where a sine-sweep over frequencies ranging from 1 Hz to 10 kHz with an amplitude of 100 mV was given to each axis using an NI PCIe-6361. The system identification yields following results for the two stages - X and Y (see Fig. 6): clearly, the positioning piezos' bandwidth

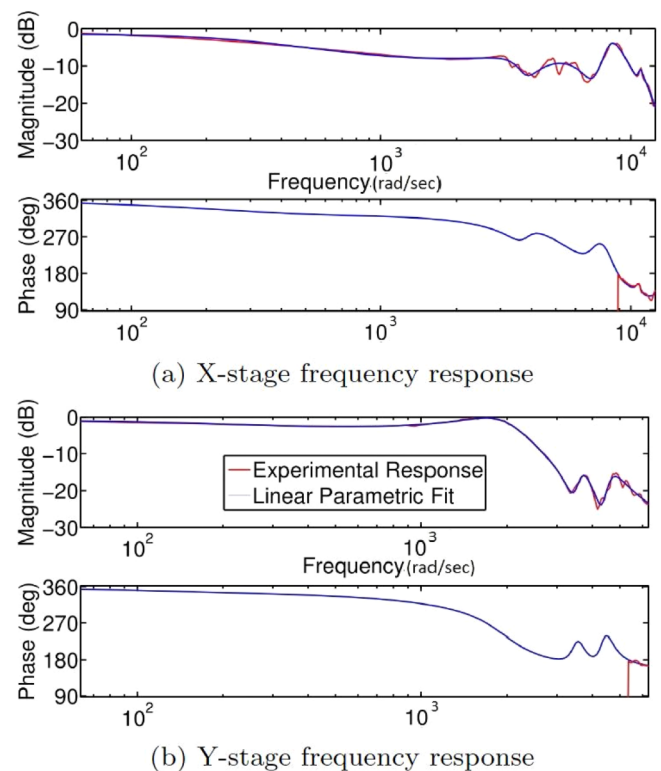


FIG. 6. Frequency response results for the piezo-stages.

is approximately 1 kHz. We are anyway not interested in the dynamics beyond this frequency regime. MATLAB `invreqs` command is used to fit a linear parametric model through the frequency response data. Weighted iterative least square fitting was performed over 0-2 kHz and the reduction through balanced realization¹¹ resulted in the following parametric models:

$$G_{xx} = \frac{-0.022119(s + 2.954 \times 10^4)(s - 8151)(s + 418.9)}{(s^2 + 717.5s + 1.013 \times 10^7)(s + 217.1)} \\ \times \frac{(s + 8117)(s^2 + 1185s + 4.616 \times 10^7)}{(s + 1796)(s^2 + 1440s + 7.142 \times 10^7)} \\ \times \frac{(s^2 + 890.2s + 1.131 \times 10^7)}{(s^2 + 1827s + 3.751 \times 10^7)} \\ \times \frac{(s^2 + 350.3s + 1.175 \times 10^8)}{(s^2 + 267.1s + 1.182 \times 10^8)} \\ \times \frac{(s^2 + 452.4s + 1.494 \times 10^8)}{(s^2 + 605.8s + 1.473 \times 10^8)},$$

$$G_{yy} = \frac{-0.054548(s^2 + 238.8s + 9.739 \times 10^5)(s - 7670)}{(s^2 + 256.3s + 8.251 \times 10^5)(s + 3158)} \\ \times \frac{(s^2 + 3179s + 1.604 \times 10^7)}{(s^2 + 522.7s + 9.055 \times 10^6)} \\ \times \frac{(s^2 + 295.3s + 1.95 \times 10^7)}{(s^2 + 438.5s + 1.891 \times 10^7)}.$$

From Fig. 6, one must note that the Y-stage is a *slower* stage and identified as a lower-order (7th-order) plant. Since the order of a plant directly determines the order of a model-based controller, implementation of optimal controller for the Y-stage is achieved using fewer FPAs. This is in contrast to the control design for higher-order X-stage, where

implementation of a full-order controller requires twice as many resources.

C. Implementation on the FPAAs

Each FPAAs board from Anadigm family has limited number of op-amps and is capable of implementing only up to a maximum of eighth-order transfer function (for non-minimum phase systems, the realized order is even lesser). However, by daisy chaining of FPAAs, higher-order controllers can be easily implemented. A full-order controller implementation requires more than one FPAAs board. The 2DOF control design schemes for lower-order Y-stage are implemented using fewer (two) FPAAs units. In addition, a 13th-order 2DOF controller is implemented on the X-stage that requires four daisy-chained FPAAs. This is in contrast to controller implementation in Ref. 18 where lack of high-speed processing capabilities in DSP did not allow simultaneous implementation of controllers for both X and Y stages. We now present the FPAAs implementation of the control algorithms described in Sec. III on the MFP-3D scanner Y-stage (and X-stage).

D. 2DOF \mathcal{H}_∞ control design for the Y-stage

To overcome the shortcomings resulting from feedback only control, we now implement a 2DOF \mathcal{H}_∞ control design, similar to Ref. 19. Even though a 2DOF framework has separate controls for reference and error signals, the fundamental algebraic limitation still holds true, $S + T = 1$. To alleviate this problem even further, weighting functions W_r and W_n are used to shape reference and noise signals, respectively. The weighting functions for the 2DOF optimization problem are

$$W_s = \frac{0.5(s + 1.257 \times 10^4)}{(s + 125.7)}, \quad W_t = \frac{58.8235(s + 1257)}{(s + 1.257 \times 10^5)}, \\ W_u = 0.1.$$

The choice of $W_r = \frac{1.9531(s+251.3)(s+5027)^2}{(s+628.3)^2(s+3.142 \times 10^4)}$ and $W_n = W_r^{-1}$ is made such that at the frequency, the W_t starts increasing, W_r starts increasing, and W_n starts decreasing (in fact, W_n is chosen as the inverse of W_r). The optimization routine resulted in the feedforward controller, K_{ff} , and feedback controller, K_{fb} , with $\gamma_{opt} = 2.8654$. Model reduction technique resulted in the following reduced-order controllers:

$$K_{ff} = \frac{-2.2489(s + 1.706 \times 10^6)(s + 1.401 \times 10^4)}{(s + 3.024 \times 10^5)(s^2 + 3052s + 4.001 \times 10^7)} \\ \times \frac{(s + 6833)(s + 2790)(s - 6764)}{(s^2 + 1.798 \times 10^4s + 3.764 \times 10^8}, \quad (8)$$

$$K_{fb} = \frac{-0.66107(s + 1.217 \times 10^5)(s + 5.997 \times 10^5)}{(s + 3.35 \times 10^5)(s + 1.219 \times 10^6)} \\ \times \frac{(s - 9.831 \times 10^6)(s^2 + 405.5s + 3.445 \times 10^6)}{(s + 4.857 \times 10^4)(s + 1.08 \times 10^4)(s + 109.4)}. \quad (9)$$

The experimental tracking results for 100 Hz triangular waveforms are shown in Fig. 7. Clearly, the 2DOF control design is better at tracking when compared to its 1DOF

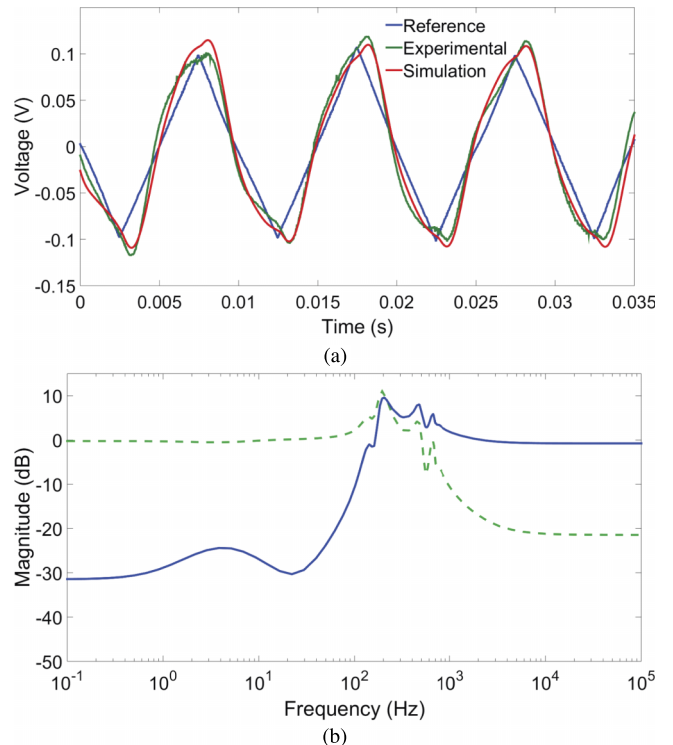


FIG. 7. 2DOF \mathcal{H}_∞ robust control for Y-stage. (a) Tracking performance for a 100 Hz triangular waveform, (b) associated *sensitivity* (solid blue) and *complementary sensitivity* (dotted green) transfer functions.

counterpart. The reference and experimental trajectories are in phase, whereas this was not the case with 1DOF setup. The closed-loop bandwidths are $\omega_B = 130$ Hz and $\omega_{BT} = 520$ Hz. The complementary sensitivity transfers function rolls-off at a rate of -20 dB/decade, thereby, attenuating high-frequency noise.

E. 2DOF model-matching control for the Y-stage

We now design the prefilter-based control, assuming K_{fb} (from 1DOF \mathcal{H}_∞ control design) as the pre-designed feedback component, where

$$K_{fb} = \frac{1.413(s + 3.607 \times 10^5)}{(s + 3.972 \times 10^4)} \frac{(s^2 + 208.1s + 7.438 \times 10^5)}{(s^2 + 168.7s + 8.335 \times 10^5)} \\ \times \frac{(s + 2150)(s^2 + 598.5s + 1.054 \times 10^7)}{(s + 125.7)(s^2 + 3479s + 2.233 \times 10^7)}. \quad (10)$$

The NP solution resulted in a stable prefilter, which after model-reduction and dc gain adjustment resulted in the following sixth-order prefilter:

$$K_{pre} = \frac{0.00079405(s + 1.217 \times 10^6)(s + 2.804 \times 10^4)}{(s^2 + 713.5s + 1.192 \times 10^6)} \\ \times \frac{(s^2 + 428.6s + 9.935 \times 10^5)}{(s^2 + 412s + 3.698 \times 10^6)} \\ \times \frac{(s^2 + 1965s + 6.623 \times 10^6)}{(s^2 + 3286s + 4.048 \times 10^7)}. \quad (11)$$

The closed-loop bandwidths are $\omega_B = 78$ Hz and $\omega_{BT} = 340$ Hz. The experimental tracking results for 100 Hz triangular waveforms are shown in Fig. 8.

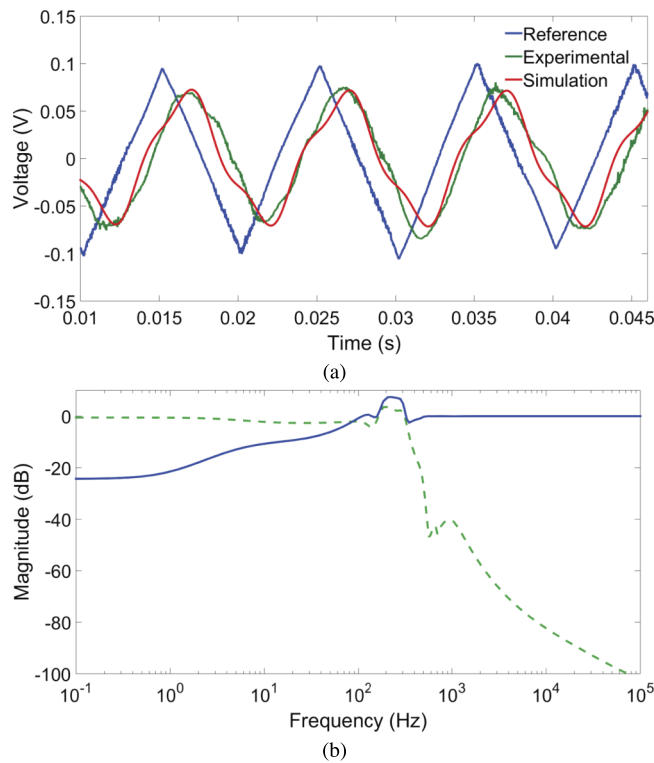


FIG. 8. Model-matching controller for Y-stage. (a) Tracking performance for a 100 Hz triangular waveform, (b) associated *sensitivity* (solid blue) and *complementary sensitivity* (dotted green) transfer functions.

F. 2DOF Optimal robust model matching control

An alternative representation of the 2DOF optimal robust model matching design is shown in Fig. 9, where W_1 is the filter for shaping the plant G , and K_1 is replaced by $K_1 W_1$ to give exact model-matching at steady-state. The parameters, ρ , W_1 , and T_{ref} can be adjusted, if required.

1. Low-order controller for Y-stage

We now implement the above 2DOF optimal robustifying model-matching controller on the Y-stage. With $\rho = 1$ and $W_1 = 1$, the optimization routine resulted in the following stabilizing controllers in the positive feedback setup:

$$\begin{aligned} K_1 &= \frac{0.29483(s^2 + 223.4s + 7.538 \times 10^5)}{(s + 7.195 \times 10^4)(s + 8701)} \\ &\quad \times \frac{(s^2 + 536.7s + 1.063 \times 10^7)}{(s^2 + 274.2s + 9.724 \times 10^5)} \\ &\quad \times \frac{(s^2 + 6.2e04s + 1.06 \times 10^{10})}{(s^2 + 1959s + 1.179 \times 10^7)}, \\ K_S &= \frac{-0.051402(s + 5902)(s + 434.7)}{(s^2 + 299.9s + 1.032 \times 10^6)} \\ &\quad \times \frac{(s^2 - 1701s + 2.723 \times 10^6)}{(s^2 + 1651s + 1.386 \times 10^7)}. \end{aligned} \quad (12)$$

The closed-loop bandwidths are $\omega_B = 116$ Hz and $\omega_{BT} = 340$ Hz. The experimental tracking results for 100 Hz triangular waveforms are shown in Fig. 10.

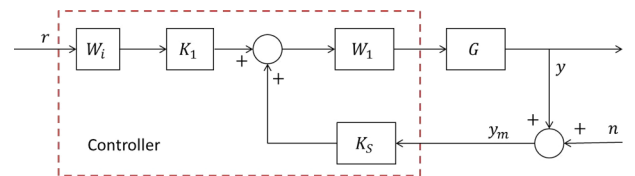


FIG. 9. Alternative representation of 2DOF Optimal robust model matching framework.

2. High-order controller for X-stage

We now implement higher-order 2DOF optimal robust model-matching controller for the X-stage. With $\rho = 1$ and $W_1 = 1$, the H_∞ optimization routine resulted in the following stabilizing controllers in the positive feedback setup:

$$\begin{aligned} K_1 &= \frac{2473622.941(s + 1935)(s + 265.2)}{(s + 1.087 \times 10^6)(s + 3336)(s + 481.3)} \\ &\quad \times \frac{(s^2 + 1897s + 3.823 \times 10^7)}{(s^2 + 9534s + 5.876 \times 10^7)} \\ &\quad \times \frac{(s^2 + 1740s + 7.089 \times 10^7)}{(s^2 + 1427s + 4.69 \times 10^7)} \\ &\quad \times \frac{(s^2 + 285.9s + 1.168 \times 10^8)}{(s^2 + 292.3s + 1.195 \times 10^8)} \\ &\quad \times \frac{(s^2 + 588.7s + 1.471 \times 10^8)}{(s^2 + 588.9s + 1.486 \times 10^8)} \\ &\quad \times \frac{(s^2 + 750.2s + 1.031 \times 10^7)}{(s^2 + 1035s + 1.117 \times 10^7)}, \end{aligned} \quad (13)$$

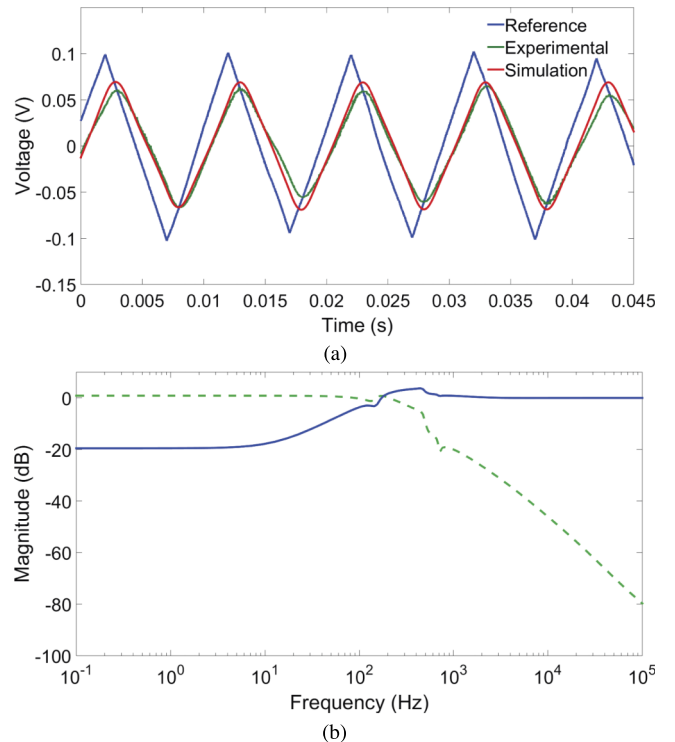


FIG. 10. 2DOF optimal robustifying model-matching control for Y-stage. (a) Tracking performance for a 100 Hz triangular waveform, (b) associated *sensitivity* (solid blue) and *complementary sensitivity* (dotted green) transfer functions.

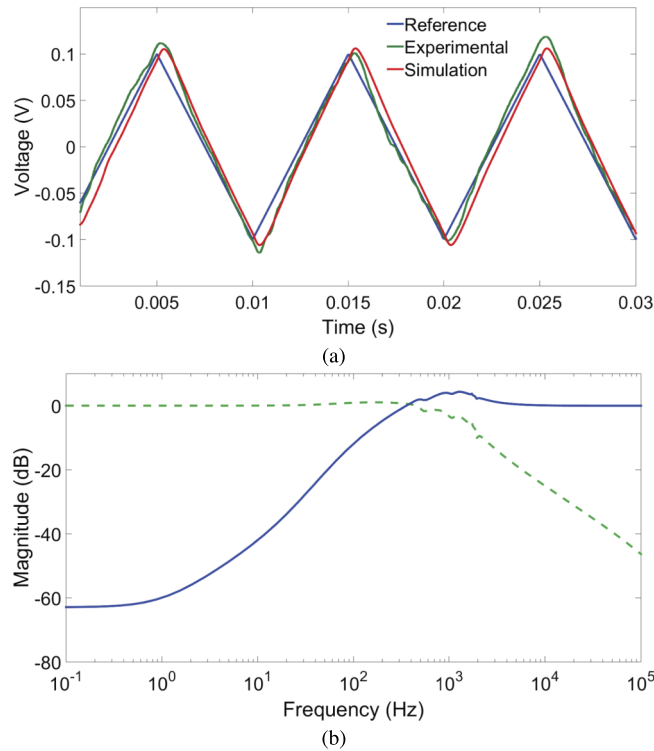


FIG. 11. 2DOF optimal robustifying model-matching control for X-stage. (a) Tracking performance for a 100 Hz triangular waveform, (b) associated sensitivity (solid blue) and complementary sensitivity (dotted green) transfer functions.

$$K_S = \frac{0.044238(s - 8.466 \times 10^6)(s + 940.8)}{(s + 1.087 \times 10^6)(s + 482.4)} \times \frac{(s^2 + 944.6s + 3.15 \times 10^7)}{(s^2 + 9588s + 5.846 \times 10^7)} \times \frac{(s^2 - 2520s + 5.961 \times 10^7)}{(s^2 + 1438s + 4.714 \times 10^7)} \times \frac{(s^2 + 201.2s + 1.181 \times 10^8)}{(s^2 + 310.7s + 1.176 \times 10^8)} \times \frac{(s^2 + 637.9s + 1.47 \times 10^8)}{(s^2 + 569.3s + 1.484 \times 10^8)} \times \frac{(s^2 + 682.2s + 8.254 \times 10^6)}{(s^2 + 1032s + 1.109 \times 10^7)}. \quad (14)$$

The experimental tracking results for 100 Hz sinusoidal and triangular waveforms are shown in Fig. 11. The closed-loop bandwidths are $\omega_B = 240$ Hz and $\omega_{BT} = 975$ Hz, which is about 200% improvement over the previously reported results¹⁹ for the 2DOF optimal robust model matching control for the X-stage. The LVDT sensor voltage to displacement gain is 7.68 $\mu\text{m}/\text{V}$. Fig. 12 shows the experimental error between commanded and observed displacements for the X-stage. It is observed that the worst case error is ~ 100 nm.

Note 1: It is evident from the above figures that the simulated and the experimental responses for both the stages are in unison. However, one may assume that the relatively poor command tracking for the Y-stage is attributed to poor control design. This however is not the case. In fact, the controllers are obtained by solving well-posed optimization problems and hence guarantee optimal closed-loop performance and

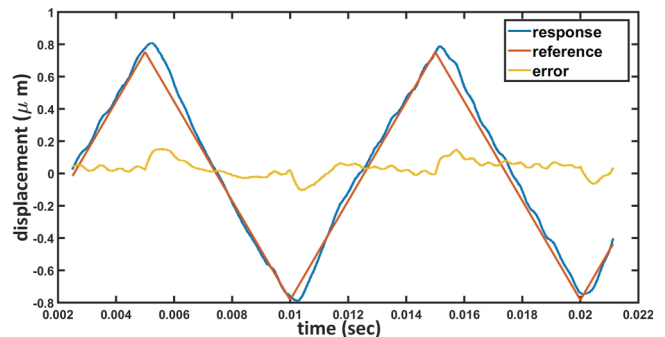


FIG. 12. Error between commanded and observed displacements for the X-stage.

robustness. From Fig. 6, it is evident that the Y-stage is a slower stage (with open-loop bandwidth ≈ 180 Hz). Hence, even with the modern control techniques, it is practically not viable for the Y-stage to completely track a band-unlimited 100 Hz triangular reference command. This however is not true for the X-stage (faster stage), where a large open-loop bandwidth (~ 370 Hz) enables high-speed tracking. We had also obtained tracking results for 20 Hz reference signal and the commanded and observed responses for the Y-stage were found to be indistinguishable; however, the low-frequency tracking results are excluded from this article for the sake of compactness.

Note 2: The definition of bandwidth in this paper is directly borrowed from the electrical engineering world and refers to -3 dB (gain ~ 0.707) crossover frequency. Since sensitivity defined earlier is a measure of lack of robustness of a closed-loop system, a -3 dB gain value in the sensitivity transfer function amounts to about 70% uncertainty. Hence, it makes sense to introduce a new definition of bandwidth for mechanical systems. We consider the -40 dB (1% uncertainty) gain crossover frequency $\omega_{B'}$. Note that for above full-order Glover-McFarlane control design, the closed-loop bandwidth with respect to -40 dB gain crossover frequency, $\omega_{B'} = \sim 80$ Hz, is comparable to the bandwidth in Ref. 18 for the same system, but defined with respect to -3 dB gain crossover. Thus the proposed implementation yields a very high degree of robustness.

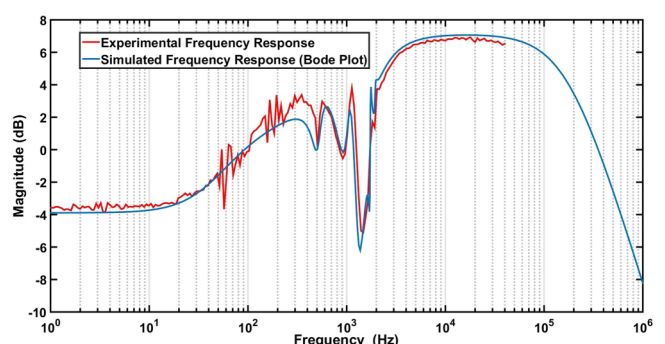


FIG. 13. Experimental frequency response of the controller K_1 . Due to the limitations of our digital signal analyzer (DSA), the identification is performed up to 40 kHz. It is clearly seen that the frequency response of the implemented controller captures various peaks in the simulated bode plot of the controller.

Note 3: The main advantage with FPAA-based control designs is the ease of implementing high-bandwidth, high-order controllers without the need to address issues such as sampling and digitization. This claim is further substantiated by obtaining the experimental frequency response of the 13th-order controller K_1 in (14) and comparing it against the simulated steady-state response, as shown in Fig. 13.

V. CONCLUSION AND FUTURE WORK

In this article, various control designs including model-matching and optimal robustifying designs have been implemented using FPAA devices and the results are found to closely match the simulated results. A significant improvement (200%) over DSP based implementations is demonstrated through experiments. Though high-speed control of nanopositioning systems is important for video-rate imaging in AFMs, faster control of cantilever systems is an equally significant and challenging requirement for AFMs. One of the future directions of this work is to extend the FPAA based implementation to achieve high-speed reference signal tracking as proposed in Ref. 24 for video rate imaging in AFM. While the experiments are being performed for model-based control of dynamic-AFMs, we have already demonstrated a successful implementation of Q-control of microcantilevers using FPAs.⁵

ACKNOWLEDGMENTS

The authors would like to acknowledge NSF grant-CMMI 14-63239 for supporting this work.

¹See <http://www.physikinstrumente.de/> for information about working principles of nanopositioning devices.

²FPAA Anadigm. Family overview. PDF File, *Anadigm*, 2003.

³T. Ando, T. Uchihashi, N. Kodera, D. Yamamoto, A. Miyagi, M. Taniguchi, and H. Yamashita, “High-speed AFM and nano-visualization of biomolecular processes,” *Pflügers Arch. Eur. J. Physiol.* **456**(1), 211–225 (2008).

⁴S. Bains, “Analog’s answer to FPGA opens field to masses,” *EE Times* **1510**, 1 (2008).

⁵M. Baranwal, Application of field programmable analog arrays (FPAs) to fast scanning probe microscopy, 2014.

⁶B. Bhikkaji, M. Ratnam, A. J. Fleming, and S. O. Reza Moheimani, “High-performance control of piezoelectric tube scanners,” *IEEE Trans. Control Syst. Technol.* **15**(5), 853–866 (2007).

⁷F. T. Calkins, R. C. Smith, and A. B. Flatau, “Energy-based hysteresis model for magnetostrictive transducers,” *IEEE Trans. Magn.* **36**(2), 429–439 (2000).

⁸D. Croft, G. Shed, and S. Devasia, “Creep, hysteresis, and vibration compensation for piezoactuators: Atomic force microscopy application,” *J. Dyn. Syst., Meas., Control* **123**(1), 35–43 (2001).

⁹A. Daniele, S. Salapaka, M. V. Salapaka, and M. Dahleh, “Piezoelectric scanners for atomic force microscopes: Design of lateral sensors, identification and control,” in *Proceedings of the American Control Conference* (IEEE, 1999), Vol. 1, pp. 253–257.

¹⁰J. C. Doyle, B. A. Francis, and A. Tannenbaum, *Feedback Control Theory* (Macmillan Publishing Company, New York, 1992), Vol. 1.

¹¹G. Dullerud and F. Paganini, *Course in Robust Control Theory* (Springer-Verlag, New York, 2000).

¹²J.-M. Galliere, “A control-systems FPAA based tutorial,” in *Proceedings of the 2nd WSEAS/IASME International Conference on Educational Technologies* (WSEAS/IASME, 2006), pp. 39–42.

¹³K. Glover and D. McFarlane, “Robust stabilization of normalized coprime factor plant descriptions with H_∞ -bounded uncertainty,” *IEEE Trans. Autom. Control* **34**(8), 821–830 (1989).

¹⁴A. G. Hatch, R. C. Smith, T. De, and M. V. Salapaka, “Construction and experimental implementation of a model-based inverse filter to attenuate hysteresis in ferroelectric transducers,” *IEEE Trans. Control Syst. Technol.* **14**(6), 1058–1069 (2006).

¹⁵S. Hauck and A. DeHon, *Reconfigurable Computing: The Theory and Practice of FPGA-based Computation* (Morgan Kaufmann, 2010).

¹⁶D. J. Hoyle, R. A. Hyde, and D. J. N. Limebeer, “An H_∞ approach to two degree of freedom design,” in *Proceedings of the 30th IEEE Conference on Decision and Control* (IEEE, 1991), pp. 1581–1585.

¹⁷K. K. Leang and S. Devasia, “Hysteresis, creep, and vibration compensation for piezoactuators: Feedback and feedforward control,” in *Proceedings of the Second IFAC Conference on Mechatronic Systems, Berkeley, CA* (IFAC, 2002), pp. 9–11.

¹⁸C. Lee and S. M. Salapaka, “Robust broadband nanopositioning: Fundamental trade-offs, analysis, and design in a two-degree-of-freedom control framework,” *Nanotechnology* **20**(3), 035501 (2009).

¹⁹C. Lee, S. M. Salapaka, and P. G. Voulgaris, “Two degree of freedom robust optimal control design using a linear matrix inequality optimization,” in *Proceedings of the 48th IEEE Conference on Decision and Control held jointly with the 28th Chinese Control Conference CDC/CCC* (IEEE, 2009), pp. 714–719.

²⁰D. J. N. Limebeer, E. M. Kasenally, and J. D. Perkins, “On the design of robust two degree of freedom controllers,” *Automatica* **29**(1), 157–168 (1993).

²¹L. Ljung, “System identification: Theory for the user,” in *Prentice Hall Information and System Sciences Series* (Prentice Hall, New Jersey, 1987), Vol. 7632.

²²MATLAB, version 7.10.0 (R2010a), The MathWorks, Inc., Natick, Massachusetts, 2010.

²³D. McFarlane and K. Glover, “A loop-shaping design procedure using H_∞ synthesis,” *IEEE Trans. Autom. Control* **37**(6), 759–769 (1992).

²⁴G. Mohan, C. Lee, and S. M. Salapaka, “High-bandwidth scanning of sample properties in atomic force microscopy,” in *ASME 5th Annual Dynamic Systems and Control Conference joint with the JSME 11th Motion and Vibration Conference* (American Society of Mechanical Engineers, 2012), pp. 561–565.

²⁵S. O. Reza Moheimani, “Invited review article: Accurate and fast nanopositioning with piezoelectric tube scanners: Emerging trends and future challenges,” *Rev. Sci. Instrum.* **79**(7), 071101 (2008).

²⁶See <http://www.innovative-dsp.com/products.php?product=p25m> for *Innovative Integration* P25M.

²⁷S. Salapaka, A. Sebastian, J. P. Cleveland, and M. V. Salapaka, “Design, identification and control of a fast nanopositioning device,” in *Proceedings of the American Control Conference* (IEEE, 2002), Vol. 3, pp. 1966–1971.

²⁸S. Salapaka, A. Sebastian, J. P. Cleveland, and M. V. Salapaka, “High bandwidth nano-positioner: A robust control approach,” *Rev. Sci. Instrum.* **73**(9), 3232–3241 (2002).

²⁹S. M. Salapaka and M. V. Salapaka, “Scanning probe microscopy,” *IEEE Control Syst.* **28**(2), 65–83 (2008).

³⁰G. Schitter, F. Allgöwer, and A. Stemmer, “A new control strategy for high-speed atomic force microscopy,” *Nanotechnology* **15**(1), 108 (2004).

³¹G. Schitter and N. Phan, “Field programmable analog array (FPA) based control of an atomic force microscope,” in *Proceedings of the American Control Conference* (IEEE, 2008), pp. 2690–2695.

³²A. Sebastian and S. M. Salapaka, “Design methodologies for robust nanopositioning,” *IEEE Trans. Control Syst. Technol.* **13**(6), 868–876 (2005).

³³S. Skogestad and I. Postlethwaite, *Multivariable Feedback Control: Analysis and Design* (Wiley, New York, 2007), Vol. 2.

³⁴M. Vidyasagar, *Control System Synthesis: A Factorization Approach* (Morgan & Claypool Publishers, 2011).

³⁵Q. Zou and S. Devasia, “Preview-based optimal inversion for output tracking: Application to scanning tunneling microscopy,” *IEEE Trans. Control Syst. Technol.* **12**(3), 375–386 (2004).